Journal of Catalysis **195,** 207–216 (2000)
doi:10.1006/jcat.2000.2981, available online at http://www.idealibrary.com on IDEAL®

Comparative Study on Redox Properties and Catalytic Behavior for CO Oxidation of CuO/CeO_2 and $CuO/ZrCeO_4$ Catalysts

A. Martínez-Arias,*,[1] M. Fernández-García,* O. Gálvez,*,[2] J. M. Coronado,* J. A. Anderson,† J. C. Conesa,* J. Soria,* and G. Munuera‡

*Instituto de Catálisis y Petroleoquímica, CSIC, Campus Universitario de Cantoblanco, Camino de Valdelatas s/n, 28049 Madrid, Spain; †Chemistry Department, University of Dundee, Dundee DD1 4HN, Scotland, United Kingdom; and ‡Departamento de Química, Inorgánica, Universidad de Sevilla, 41092 Sevilla, Spain

Received April 27, 2000; revised June 23, 2000; accepted June 27, 2000

Redox processes occurring during the CO–O_2 reaction and catalytic properties for CO oxidation have been examined for CuO/CeO_2 and $CuO/ZrCeO_4$ catalysts using catalytic activity tests, *in situ* **DRIFTS and EPR spectroscopies, and CO-TPD. EPR results suggest synergetic effects in the reduction–oxidation of these systems, both copper and the support being involved in these redox processes. Both EPR and CO-TPD experiments indicate a more facile reduction by CO of the CuO/CeO_2 system, mainly due to the greater reducibility of sites at the interface between the copper oxide clusters and the support for this catalyst. A greater CO oxidation activity is exhibited by the CuO/CeO_2 catalyst. A comparison of both catalysts and analysis of the redox properties of the different copper entities present in the catalysts indicate that the active copper sites for CO oxidation are located on the copper oxide clusters. On the basis of the results obtained by the different techniques, it is proposed that CO oxidation in these systems follows a redox mechanism in which both the support and copper oxide clusters are simultaneously reduced or oxidized following interaction with CO or O_2, respectively. The limiting step in the reaction is related to the oxidation process.**

Key Words: **CuO/CeO_2 and $CuO/ZrCeO_4$ catalysts; CO oxidation;** *in situ* **DRIFTS; EPR; CO-TPD.**

INTRODUCTION

Cerium oxide has traditionally been used as a promoter in the so-called "three-way catalysts" (TWCs) employed for the control of toxic emissions from automobile exhausts (1). The promoting roles of cerium oxide are proposed to involve multiple processes such as the enhancement of the noble metal dispersion and the stabilization of the support toward thermal sintering (2), as well as its direct participation in chemical processes like the water–gas shift reaction (3) or the decomposition of nitrogen oxides (4), and in general, processes involving incorporation/removal of structural oxygen, which are denoted as the oxygen storage capacity (OSC) of the system (5). In recent studies, it has been shown that the redox behavior of cerium oxide can be severely modified by incorporation of zirconium and the formation of mixed Zr–Ce oxides (6–11). A remarkable enhancement of the bulk cerium reduction is produced in these mixed oxide materials, compared with pure ceria (7, 12, 13), especially when the materials have been previously subjected to redox cycles in H_2 at high temperature (ca. 1273 K) and O_2 at relatively low temperature (less than ca. 823 K) (7). This allows a large OSC to be maintained in the system after having been thermally sintered, in contrast to pure CeO_2. Among the possible compositions and phases forming Zr–Ce mixed oxides, it has been shown (14) that the greatest promoting effect on cerium reduction is produced for compositions with Ce/Zr (atomic ratio) close to 1, and in the presence of a pseudocubic phase t″ (with Zr and Ce cations occupying the corresponding positions in the cubic fluorite-type lattice, but with overall tetragonal symmetry due to oxygen displacement from the ideal fluorite sites (7, 15, 16)).

Recent reports have shown that the activity of Ce-related oxides in complete oxidation reactions is greatly enhanced not only by noble metals (Rh, Pt, and/or Pd) (1, 6, 12), which generally form part of the TWCs, but also by base metals like copper (13, 17–19). The promoting effect has been correlated with the synergism of the redox properties of the system, which is achieved by the formation of copper–ceria interactions, with both components being significantly more readily reduced or oxidized than the corresponding independent components (18, 20). In a study involving CuO/CeO_2 samples of different copper loadings, a correlation was observed between the amount and reducibility of well-dispersed CuO entities and the catalytic activity for CO oxidation. This led to the conclusion that these well-dispersed CuO entities contain the active sites

[1] To whom correspondence should be addressed. E-mail: amartinez@icp.csic.es.

[2] Present address: Departamento de Química-Física, Facultad de Química, Universidad Complutense, 28040 Madrid, Spain.

0021-9517/00 $35.00

for low-temperature CO oxidation, unlike lesser dispersed CuO entities that show lower reducibility (18). Liu *et al.* (17) also proposed that copper entities active for the reaction involved small oxidized copper clusters. More recently, it has been demonstrated that redox processes in ceria-supported copper materials involve reduction and oxidation of both the copper and ceria species, both components acting together (20). Other factors that can influence the catalytic activity of these systems include the structure sensitivity of CO oxidation in these catalysts (21).

When comparing ceria and cerium–zirconium mixed oxide supports for copper catalysts, a recent report (22) showed lower CO oxidation activity for the catalyst supported on the mixed oxide, which was attributed to the more facile reduction–oxidation of copper entities in the ceria-supported catalyst. However, since the catalysts were presumed to present significantly different copper dispersions (due to differences in the specific areas of the supports), a comparison between results was inconclusive (22). The objective of the present work was to determine the nature of aspects that would explain the light-off behavior for CO oxidation in this type of system. For this purpose, and in the context outlined above, two copper catalysts supported on CeO_2 and $ZrCeO_4$ supports of comparable areas were studied with regard to their redox and catalytic properties.

EXPERIMENTAL

Materials. A high surface area ($96\,m^2\,g^{-1}$) Zr–Ce (atomic ratio 1 : 1) mixed oxide was used as one of the supports. It was prepared by a microemulsion–coprecipitation method by mixing two reverse microemulsions containing aqueous phases prepared by dissolving similar amounts (0.25 M) of cerium(III) nitrate hexahydrate and zirconyl nitrate for the first and tetramethylammonium hydroxyde pentahydrate (1.5 M) for the second, dispersed in an organic solvent (*n*-heptane), using Triton X-100 (Aldrich) as the surfactant and hexanol as the co-surfactant. The weight percentages of the aqueous solution, organic solvent, surfactant, and co-surfactant employed for preparing these microemulsions were, respectively, 8, 58, 15, and 19. Following centrifugation, decanting, and rinsing of the resulting solid with methanol, it was dried at 383 K for 24 h and finally calcined in air at 773 K for 2 h. More details on the preparation of this support can be found elsewhere (23). In the case of the Zr–Ce mixed oxide obtained, a thorough precipitation of both cerium and zirconium components was achieved (on the basis of ICP-AES analysis of the final product), while the material consisted of ca. 5-nm crystallites (based on TEM results; XRD estimation of the particle size showed good agreement with the TEM observation), presenting the pseudocubic phase t″ (on the basis of XRD and Raman analyses) and showing a good compositional homogeneity (23). The CeO_2 support was prepared by a similar method and showed $S_{BET} = 72\ m^2\,g^{-1}$. XRD and Raman experiments showed the presence of the fluorite structure for this support. XRD estimation of the crystallite size for this solid indicated a larger size (ca. 8.5 nm) than that found for the mixed oxide support.

Samples of copper supported on $ZrCeO_4$ and CeO_2 (referred to as CuZC and CuC, respectively) were prepared by impregnation of the above-mentioned supports using aqueous solutions of $Cu(NO_3)_2 \cdot 3H_2O$ (to give a final copper load of 1 wt%, representing ca. 157 μmol of Cu/g of catalyst). The resulting materials were dried overnight at 383 K and subsequently calcined in air at 773 K for 2 h. XRD analyses of the supported copper samples showed only peaks similar to those observed for the copper-free supports.

All the gases employed were of commercial purity and, for experiments using the vacuum line (EPR experiments), were further purified by vacuum distillation, before storage.

Techniques. EPR spectra were recorded at 77 K with a Bruker ER 200 D spectrometer operating in the X-band and calibrated with a DPPH standard ($g = 2.0036$). Portions of about 50 mg of sample were placed inside a quartz probe cell with greaseless stopcocks using a conventional high-vacuum line (capable of maintaining a dynamic vacuum of ca. $6 \times 10^{-3}\ N\,m^{-2}$) for the different treatments. In all cases, the samples were pretreated in 300 Torr of pure oxygen at 773 K for 2 h. Except where specified, CO reduction treatments at a specific reduction temperature (T_r) were made under static conditions using 100 Torr of CO, heating for 1 h at the corresponding T_r, and subsequently outgassing at the same temperature for 0.5 h. Quantitative evaluation of the amount of species present in the spectra was performed by double integration of the corresponding EPR spectra and comparison with a copper sulfate standard. Computer simulations were used when necessary to determine spectral parameters.

Catalytic tests were carried out using a fixed-bed glass flow reactor system equipped with a coaxial thermocouple for measuring the temperature profiles at the catalyst bed and loaded with ca. 3 g of sample. Analysis of the feed and outlet gas streams was performed using a Perkin-Elmer FTIR spectrometer model 1725X, coupled to a multiple reflection transmission cell (Infrared Analysis Inc. "long path gas minicell," 2.4-m path length, ca. 130-cm^3 internal volume); O_2 was determined with a paramagnetic analyzer (Servomex 540 A). Prior to catalytic testing, the catalysts were subjected to a standard calcination pretreatment using 3% O_2/N_2 flow at 773 K for 1 h, cooling to room temperature (RT) in the same flow, and finally briefly purging in N_2. The CO oxidation catalytic tests were performed under stoichiometric conditions in 1% CO and 0.5% O_2 in N_2 at a fixed space velocity of $3 \times 10^4\ h^{-1}$ (roughly corresponding to $0.18\ g\,s\,cm^{-3}$ contact time for both catalysts). In all cases, the runs were commenced after an initial equilibration period of ca. 5 min in the reactant flow.

DRIFTS analysis of the catalyst surface under reaction conditions was performed using a Perkin-Elmer 1750 FTIR spectrometer equipped with an MCT detector. The DRIFTS cell (Harrick) was fitted with CaF_2 windows and a heating cartridge, which allowed samples to be heated to 773 K. Samples of ca. 80 mg were calcined *in situ* (in a similar manner to the catalytic activity tests) and then cooled to room temperature before the reaction mixture consisting of 1% CO and 0.5% O_2 in N_2 was introduced and a total flow of ca. 80 $cm^3\ min^{-1}$ was used. A pc controlled gas blender was used to control the composition of the inlet gases.

CO-TPD experiments were performed with a VG 100-D Balzers mass spectrometer, monitoring the m/z ratios 12 (C), 28 (CO), 40 (Ar), and 44 (CO_2). Portions of ca. 120 mg of used catalysts (after the catalytic activity tests in stoichiometric $CO:O_2$ up to 473 K) were calcined *in situ* at 773 K under a flow (80 $cm^3\ min^{-1}$) of $O_2:Ar = 1:3$. After the sample was cooled to RT in the gas flow, it was purged extensively in Ar and then exposed to $CO:Ar$ (1:4) at that temperature for 10 min. Finally, the sample was first purged extensively (90 min) under Ar at RT and then the temperature was raised under Ar using a ramp of 10 K min^{-1} and a flow of 50 $cm^3\ min^{-1}$.

RESULTS

$CO + O_2$ Catalytic Activity Tests

Results of light-off tests for the two catalysts are shown in Fig. 1. The profiles reveal the higher activity of CuC, which shows significant activity even from RT, presenting overall ca. 30 K lower iso-conversion temperatures than CuZC. The latter shows a large activity increase at 353 K, although it exhibits a certain activity also at lower temperatures. It is worth noting that the first few points at lower temperature can be affected to a certain degree by CO adsorption phenomena rather than by actual CO conversion to gaseous CO_2 since $[CO]+[CO_2]$ at the reactor outlet was slightly lower than 1% (the value of $[CO]_{inlet}$) for those points. Similar reactivity profiles were obtained when the catalysts were calcined in 3% O_2/N_2 at 773 K at the end of the runs.

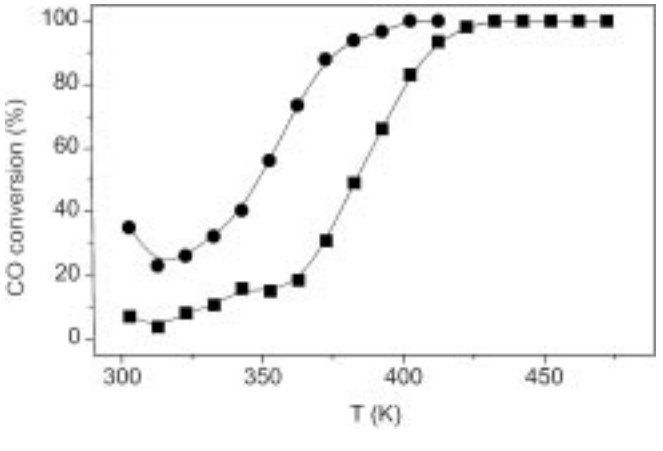

FIG. 1. CO oxidation activity on CuC (circles) and CuZC (squares).

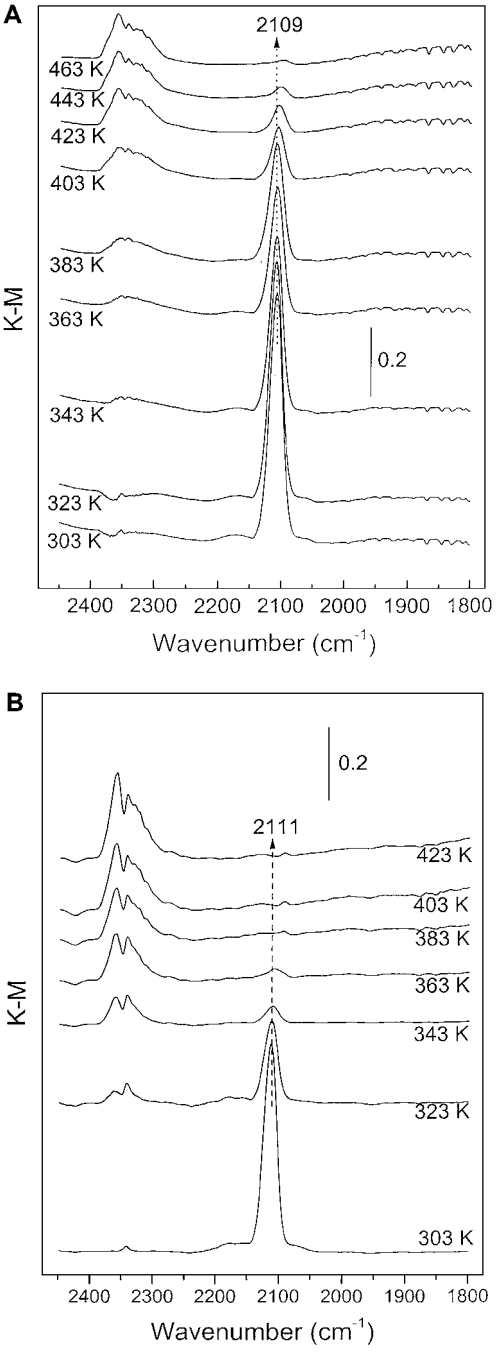

FIG. 2. DRIFT spectra obtained in reaction conditions (stoichiometric $CO–O_2$ in N_2 flow) for (A) CuZC and (B) CuC at the indicated temperatures.

FTIR Experiments

DRIFT spectra recorded under reaction conditions at increasing temperature (Fig. 2) indicate a progressive

decrease in CO gas contribution (appearing as relatively broad bands in the 2200- to 2050-cm^{-1} region) and an increase in CO_2 gas (band envelope at ca. 2350 cm^{-1}), in general correlation with light-off plots (Fig. 1). Additionally, a carbonyl band at ca. 2110 cm^{-1}, whose intensity decreased and showed a certain red shift with increasing reaction temperature, was observed for both catalysts. A comparison of band intensities for both samples at iso-conversion temperatures show, in general, a higher intensity for sample CuZC. For example, compare the spectra for $T = 383$ K in Fig. 2A and $T = 343$ K in Fig. 2B which shows both ca. 40% gaseous CO_2 with respect to the value obtained at 100% conversion.

Following the runs in CO-O_2 up to 473 K, the samples were cooled in an inert gas flow to RT, after which 1% CO flowed through the cell and a spectrum was recorded. As shown in Fig. 3a, the band at ca. 2110 cm^{-1} reappears for both catalysts. It shows a relatively high intensity in both cases, although it is slightly lower for sample CuC. The thermal stability of this carbonyl was checked by recording spectra at increasing temperatures under an inert gas flow. As shown in Figs. 3b–3e, the carbonyl on CuC shows a lower stability as it had almost completely disappeared at 348 K, while for CuZC, ca. 30% of its initial intensity remained at 373 K. A small increase in bands appearing in the 1700- to 800-cm^{-1} range (not shown), due to adsorbed CO_x (carbonate or carboxylate species (1)) was observed with increasing temperature (up to 373 K) in these experiments. Additionally, a small increase in the CO_2 gas contribution was observed with increasing temperature under the inert flow in these experiments.

The frequency of the copper carbonyl is often used to identify the oxidation state and structural nature of the adsorption center (20, 24–27). It is generally acknowledged that carbonyl bands at wavenumbers lower than ca. 2115 cm^{-1} are due to carbonyl species adsorbed on metallic copper particles while those at higher wavenumber correspond to carbonyls adsorbed on oxidized copper sites, the wavenumber increasing with the copper oxidation state. Variations in the frequency of these carbonyls have been related to changes in the nature of the exposed faces (i.e., in the degree of coordination of the copper centers). Additionally, in the case of supported catalysts, metal–support interactions must be considered as these can produce frequency shifts with respect to the values obtained on unsupported metals (20, 25, 26). Another means of identifying the nature of the adsorption centers is based on the relative strengths of the CO–copper bonds. For species presenting overlapping bands, Cu^+ carbonyls usually show significantly higher thermal stability than Cu^0 or Cu^{2+} carbonyls and thus usually withstand RT outgassing, while the others would readily undergo desorption under the same conditions (27). Another aspect to consider while interpreting these spectra concerns the extinction coefficients of the carbonyls, which are usually higher for Cu^+ carbonyls than for Cu^0 carbonyls (28). The band at ca. 2110 cm^{-1} lies at the limit of the range of frequencies, which may be assigned to carbonyls adsorbed on metallic copper particles (24). However, the high thermal resistance of the carbonyls under inert gas

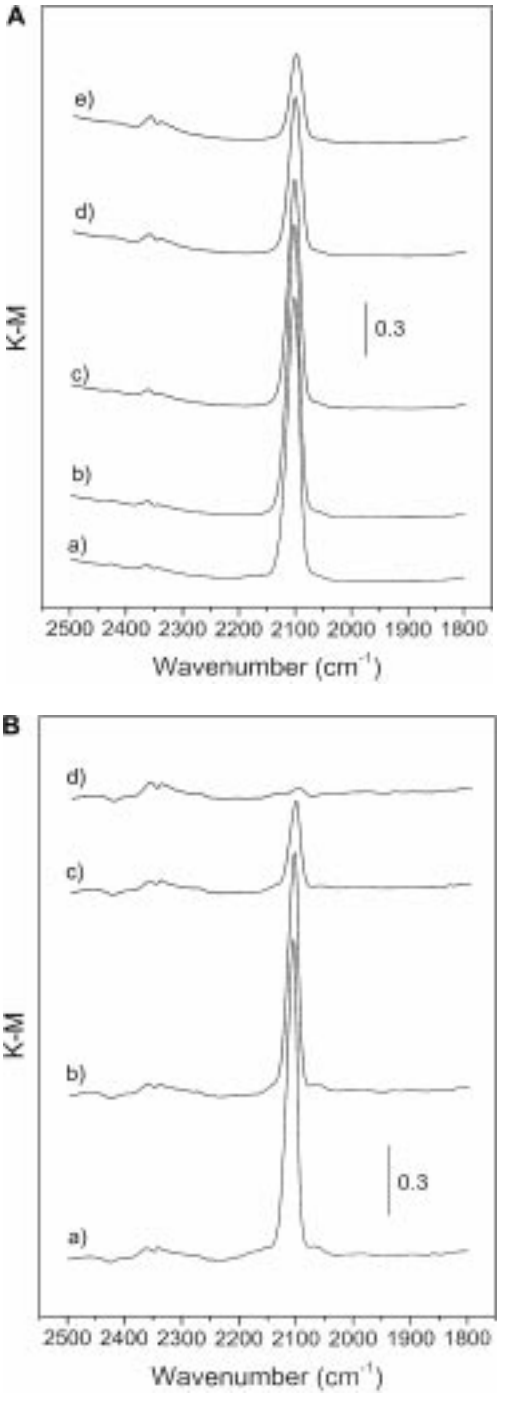

FIG. 3. DRIFT spectra obtained after CO–O_2 reaction up to 473 K and cooling to RT under an inert gas flow for (A) CuZC and (B) CuC. (a) Spectrum taken under 1% CO/N_2 flow at RT. Spectra taken after subsequent treatment under N_2 flow at (b) RT, (c) 323 K, (d) 348 K, and (e) 373 K.

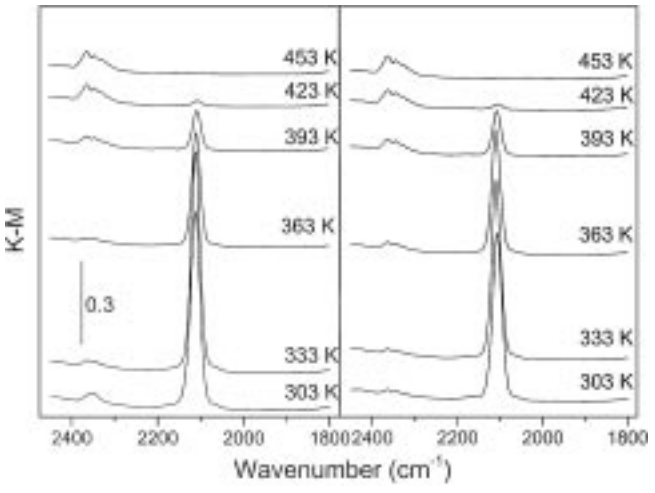

FIG. 4. DRIFTS results of consecutive reaction tests in stoichiometric $CO–O_2$ reaction conditions with intermediate cooling under an inert gas flow obtained for CuZC at the indicated temperatures. Left, 1st run; right, 2nd run.

flow, along with the fact that they usually show maximum intensity at relatively low reduction temperatures (considering overall conditions in which no strong copper sintering is produced) (20), strongly suggests that the adsorption center is in an oxidized state, likely Cu^+ (19, 20, 26).

Further DRIFTS experiments were performed using CuZC to investigate whether the catalytic or surface properties of the catalyst changed as a consequence of exposure to the reactant gases. To check this, two consecutive reaction tests with an intermediate cooling to RT in an inert gas flow were performed. The almost identical spectra obtained in both tests (Fig. 4) suggests that no important modifications occurred.

CO-TPD

The CO-TPD profiles observed for both samples following CO adsorption at RT on used samples followed by calcination (see Experimental part) are shown in Fig. 5. A significant portion of the CO is desorbed as CO_2 in both samples, although the ratio of desorbed CO_2/CO is apparently higher for CuC. For CuC, CO_2 desorption gives a rather symmetric peak at 390 K, which initiates from RT and shows a tail extending up to 723 K (where the experiment was stopped). On the other hand, CO_2 desorption from CuZC was shifted to a higher temperature and showed a broader peak with a maximum at 415 K with a longer tail to high temperatures. Differences were also observed in the CO desorption profiles of both samples. While CuZC showed a peak at 325 K and a broad one extending from ca. 390 to 723 K (with a maximum at ca. 480 K), CO desorbed mainly in a peak at 346 K for CuC.

EPR

Figure 6A shows EPR spectra of the initial calcined samples after reduction in CO at $T_r = RT$ and 373 K. Evolution of the overall intensity of the spectra with T_r is shown in Fig. 6B. The spectra of the initial calcined samples are formed by the overlapping of different signals: A major featureless broad signal showing extremes at $g =$ 2.23–2.20 and $g = 2.04$, signal B, and other axial signals in which four-line hyperfine splittings can be resolved in each of its components (signals type C). Only subtle differences are appreciated in the characteristics of signal B appearing in each sample; it apparently presents a slightly higher width for CuZC than for CuC. Two signals can be discerned among type C's appearing for sample CuC. They show $g_\parallel = 2.233$ ($A_\parallel = 16.0 \times 10^{-3}$ cm^{-1}) and $g_\perp = 2.036$ ($A_\perp = 1.8 \times 10^{-3}$ cm^{-1}), signal C1, and $g_\parallel = 2.274$ ($A_\parallel = 17.4 \times 10^{-3}$ cm^{-1}) and $g_\perp = 2.041$ ($A_\perp = 2.3 \times 10^{-3}$cm^{-1}), signal C2. Analysis of the hyperfine splitting features superimposed on the profile of signal B in the spectrum of the calcined sample CuZC shows that a signal of type C1 is also present in this sample, although it shows somewhat larger linewidth. The main difference observed between samples in the evolution of the signals following reduction involves a significantly greater decrease of signal B in the case of CuC, this fact being most determinant in explaining the differences observed in the evolution of the overall intensities of the spectra (Fig. 6B). A significant decrease of this signal is produced in sample CuC, even after reduction at $T_r = RT$, and only a small-signal type C (along with a minor signal characterized by a hyperfine splitting giving rise to six symmetric signals centered at $g = 2.00$ and with $A = 8.7 \times 10^{-3}$ cm^{-1}, typical of Mn^{2+} impurities usually present at the ppm level in the precursors employed to prepare the cerium-containing catalysts) is present after reduction at $T_r = 373$ K. However, for sample CuZC,

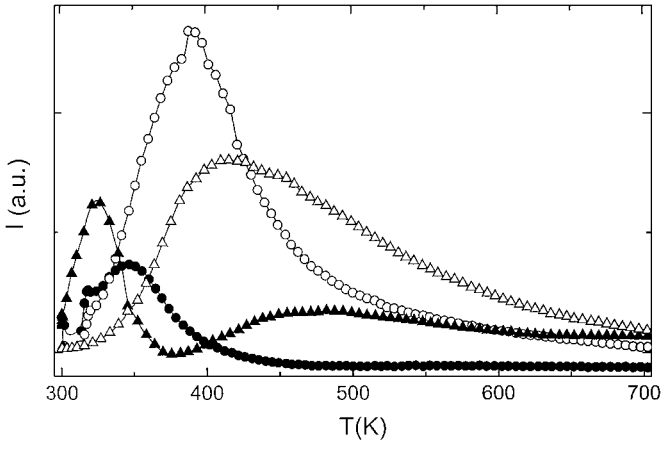

FIG. 5. CO-TPD results obtained over used catalysts precalcined at 773 K. CuZC (triangles) and CuC (circles). Full symbols, $m/e = 28$; open symbols, $m/e = 44$.

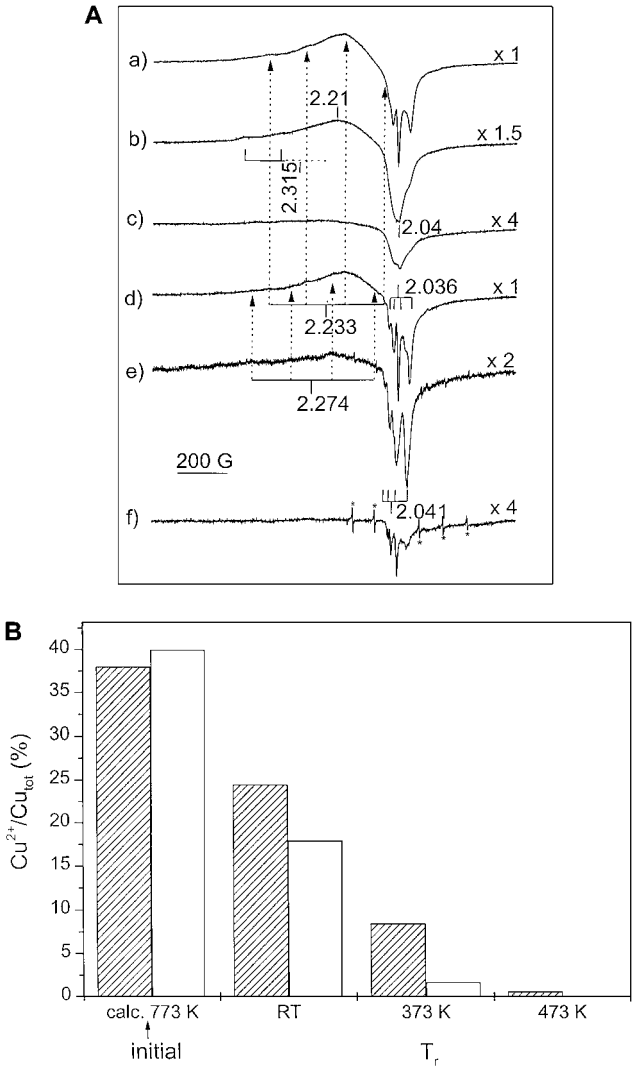

FIG. 6. (A) EPR spectra of (a) initial calcined CuZC, (b) CuZC reduced in CO at $T_r = RT$, (c) CuZC reduced at $T_r = 373$ K, (d) initial calcined CuC, (e) CuC reduced in CO at $T_r = RT$, and (f) CuC reduced at $T_r = 373$ K. (B) Overall Cu^{2+} intensity detected by EPR for the initial calcined samples and after reduction in CO at the indicated T_r. White, CuC; hatched, CuZC.

signal B shows a comparatively smaller decrease upon reduction at $T_r = RT$, gradually decreasing with increasing T_r, although a small amount of this signal is still present after reduction at $T_r = 373$ K. In both samples, signal C1 decreases strongly after contact with CO, even at $T_r = RT$. This allows improved differentiation of the features of the other signal type C present in sample CuC (signal C2). In the case of sample CuZC, the presence of another signal type C is observed following this reduction treatment, for which only the two first hyperfine features (at lower field) of the parallel component are discerned, from which a $g_{\|}$ value of 2.315 with $A_{\|} = 15.5 \times 10^{-3}\ cm^{-1}$ is obtained, signal C3. Both signals C2 (in the case of sample CuC) and C3 (for CuZC) show a large decrease after treatment at $T_r = 373$ K.

Type C signals are typical of isolated Cu^{2+} ions, their different EPR parameters reflecting differences in the coordination environments of the corresponding ions, which are consistent with increasing degrees of coordinative unsaturation in the order C3 < C2 < C1 (20, 30). Signal B, showing average $\langle g \rangle$ values close to those of type C signals, must also be due to Cu^{2+} ions; its larger linewidth (leading to unresolved hyperfine splitting) can be attributed to dipolar broadening effects caused by mutual interactions between paramagnetic Cu^{2+} ions, indicating that the corresponding ions are located in a Cu^{2+}-containing aggregated phase of an oxidic type (20). Taking into account that antiferromagnetic couplings between Cu^{2+} ions in well-crystallized CuO phases produce EPR-silent species (31), Cu^{2+} ions yielding signal B can be considered as belonging to small copper oxide clusters, while relatively larger copper oxide particles would also be present in both samples, accounting for the portion of copper that is undetected in the initially calcined samples (Fig. 6B). Similar conclusions were reached in a previous report for another Cu/CeO_2 sample on the basis of combined EPR–XPS experiments (20).

Experiments of oxygen adsorption at low temperature (77 K, RT) have been performed on the samples reduced in CO to gain insight into redox processes occurring both at the support and at copper components of the samples (20, 23, 32). Figure 7 shows experiments performed on samples reduced in CO at $T_r = RT$, at which a lesser

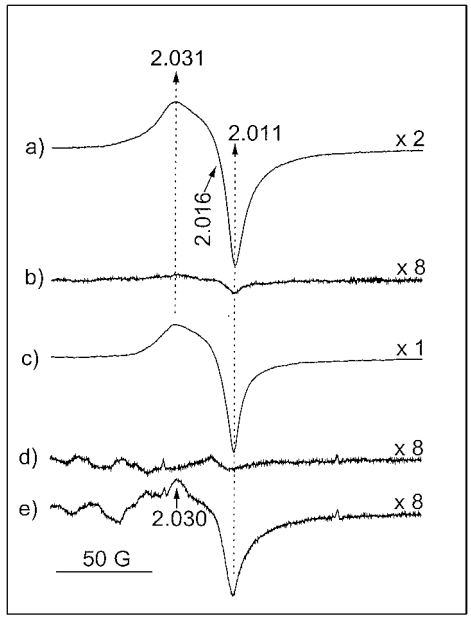

FIG. 7. EPR spectra following oxygen adsorption on the catalysts reduced in CO at $T_r = RT$: (a) 70 μmol g^{-1} adsorbed at 77 K (followed by outgassing at 77 K) on CuZC; (b) subsequent warming to RT; (c) 70 μmol g^{-1} adsorbed at 77 K (followed by outgassing at 77 K) on CuC; (d) subsequent warming to RT; (e) subsequent adsorption of 70 μmol g^{-1} at 77 K (followed by outgassing at 77 K). In all cases, contributions of Cu^{2+} signals have been cancelled by computer subtraction operations.

difference in the degree of copper reduction, compared to higher T_r, is observed (Fig. 6B) while only CuC is active for CO oxidation at that temperature (Fig. 1). As shown in Fig. 7a, an orthorhombic signal at $g_z = 2.031$, $g_x = 2.016$, and $g_y = 2.011$ (axes assignment following previous conventions (32)), due to superoxide species bonded to cerium ions (formally O_2^-–Ce^{4+}) (20, 23, 32), appears upon oxygen adsorption (70 μmol g^{-1}) at 77 K (followed by outgassing at 77 K) on CuZC. This signal shows a significant decrease upon subsequent warming to RT, although it can still be detected after this treatment (Fig. 7b). No important changes were observed in this signal when 70 μmol g^{-1} additional O_2 were introduced at 77 K (followed by outgassing at 77 K) or after subsequent warming to RT. In the case of sample CuC, parallel experiments show formation of a similar O_2^-–Ce^{4+} signal after the first adsorption at 77 K (Fig. 7c). In contrast to the behavior observed for sample CuZC, this signal completely disappeared after subsequent warming at RT (Fig. 7d) and partially reappeared after subsequent adsorption of 70 μmol g^{-1} at 77 K (Fig. 7e), again disappearing after warming to RT.

At the end of these O_2 adsorption experiments, the Cu^{2+} intensity shown by the initial calcined samples was recovered in both samples. Details of this copper re-oxidation process for sample CuC are shown in Fig. 8. The spectra show that copper in copper oxide clusters was easily re-oxidized by oxygen at RT, giving rise to a full recovery of signal B.

O_2^-–Ce^{4+} species also exhibit a higher stability in CuZC when comparing more reduced samples (at $T_r = 373$ K). Following oxygen adsorption experiments at 77 K–RT similar to those described above (results not shown), those species show a relatively high intensity in both samples after adsorption of 70 μmol g^{-1}, disappearing completely in sample CuC after 20 min of warming to RT while a small amount of O_2^-–Ce^{4+} was still present after the same treatment in CuZC.

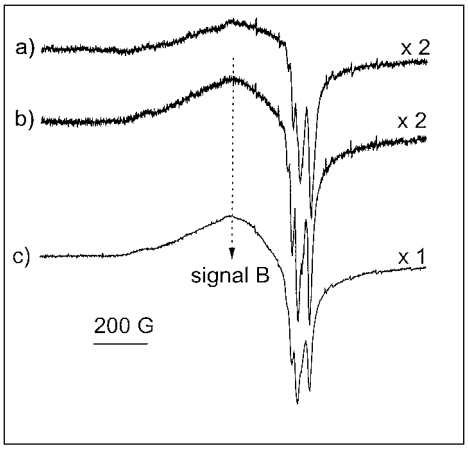

FIG. 8. (a) EPR spectrum of CuC reduced in CO at $T_r = RT$. EPR spectra after subsequent O_2 adsorption: (b) 70 μmol g^{-1} adsorbed at 77 K (followed by outgassing at 77 K), subsequent warming to RT and outgassing at RT. (c) Following the same process after subsequent adsorption of 70 μmol g^{-1} additional oxygen.

DISCUSSION

As outlined in the Introduction, a correlation between the catalytic activity for CO oxidation and the redox properties of this kind of catalysts is expected according to previous studies (18, 20). In the present case, a similar correlation can be established when comparing Cu^{2+} reducibility (Fig. 6B) and catalytic activity (Fig. 1). Furthermore, analysis of the EPR spectra of Fig. 6A shows that the species which are mainly involved in explaining the different reducibility of both samples are Cu^{2+} ions belonging to copper oxide clusters (signal B), which are more easily reduced for CuC than for CuZC. Those sites are also easily re-oxidized (Fig. 8). These results strongly suggest that the copper entities active for CO oxidation in these samples correspond to the copper oxide clusters, in agreement with previous proposals (17, 18). It is worth noting that the isolated Cu^{2+} cations with the higher degree of coordinative unsaturation (signal C1) can also be reduced by CO at RT. However, the fact that no important difference in behavior between both samples is observed in the reduction of such centers and that they represent a very small amount of the whole copper present in the samples suggests that they are not important in explaining the different catalytic behavior. They may, however, make a certain contribution to activity at $T < 353$ K for sample CuZC (Fig. 1).

EPR results of oxygen adsorption show that redox changes occurring following interaction of the samples with CO–O_2 affects not only the copper but also the supports. The observation of O_2^-–Ce^{4+} when oxygen is adsorbed on the samples reduced in CO at $T_r = RT$ indicates the generation of oxygen vacancies and reduced cerium centers for such a reduction treatment. The relatively low T_r at which the supports are reduced shows the synergetic effect of copper on their reduction (20), suggesting in turn that the reduced centers are located at interface positions. Indeed, the parameters of the O_2^-–Ce^{4+} signal obtained are close to those observed for samples of palladium dispersed on ceria-based supports and attributed to species located at interface sites (33). On the other hand, the strong decrease or disappearance of the signal after warming to RT, along with the absence of its formation (or only partial recovery) upon adsorption of a second dose of oxygen, indicates that those support sites at the interface can be strongly oxidized by O_2 at RT, this interaction yielding diamagnetic species (peroxide or oxide anions). Following these arguments, observation of a greater amount of O_2^-–Ce^{4+} after oxygen adsorption on CuC reduced at $T_r = RT$, compared to CuZC (Fig. 7), indicates that a greater extent of support surface reduction is produced in the former.

The fact that a higher copper reduction is also achieved for CuC strongly supports the existence of synergetic interactions between copper and the supports to explain the redox behavior of these systems, indicating again that sites which are involved in these processes must be located at copper–support interface positions.

The greater reducibility of the CuC system is also inferred from the lower temperature of the CO_2 desorption peak observed in the TPD experiment for that catalyst (Fig. 5). Analysis of TPD results (Fig. 5) indicates that CO desorption follows two different paths for both samples. A small amount desorbs as CO at low temperature while, in agreement with a previous report (18), the main part desorbs as CO_2 at higher temperature. A correlation can be established in qualitative terms between these results and IR ones (Fig. 3) if the lower stability of Cu^+ carbonyls in sample CuC is related to the main desorption path involving CO_2 formation. This probably occurs through interaction of those carbonyls with interface oxide anions, leading to further progress in the interface reduction process with generation of metallic copper. It is important noting that when examining jointly TPD and IR results of Figs. 3 and 5, there could be small differences in the copper oxidation states at the beginning of each experiment. As discussed below when considering interaction of the catalysts with the reactant mixture, the CuZC catalyst probably starts from a slightly more reduced state for the IR experiments (Fig. 3) while, in contrast, CuC is slightly more reduced at the beginning of the TPD experiments (Fig. 5), according to EPR results (Fig. 6B). On the other hand, the large CO_2 desorption tails observed at high temperature in the TPD experiments (Fig. 5) for both catalysts can be related to desorption of adsorbed CO_x species (1).

The facile reduction–oxidation of both copper oxide clusters and the support at interface positions following interaction with $CO–O_2$ implicates a redox mechanism for CO oxidation in these systems, during which both components of the catalyst acting together are oscillating between reduced and oxidized states. In a previous study using another CuO/CeO_2 sample, generation of Cu^+ carbonyls upon CO adsorption at RT was observed as a consequence of the reduction process and not of the presence of Cu^+ ions in the initial calcined sample (20). It seems reasonable, therefore, to assume that copper in the initial calcined samples is in a fully oxidized state. The results obtained are consistent with the existence of a first reaction step involving reduction with CO (and concomitant CO_2 evolution), leading to generation of mainly Cu^+ and Ce^{3+} entities with doubly ionized oxygen vacancies being created at the interface between copper oxide clusters and the support:

$$Ce^{4+}–O^{2-}–Cu^{2+} + CO \rightarrow Ce^{3+}–V_{\ddot{O}}–Cu^{+} + CO_2. \quad [1]$$

According to DRIFTS results and catalytic tests showing the existence of CO chemisorption at low temperatures, carbonyl species (band at ca. 2110 cm^{-1}) can be formed upon CO adsorption on those reduced centers:

$$Ce^{3+}–V_{\ddot{O}}–Cu^{+} + CO \rightarrow Ce^{3+}–V_{\ddot{O}}–Cu^{+}–CO. \quad [2]$$

At this stage, the system could evolve by a reductive process by interaction of the carbonyl species with interface sites, increasing the degree of interface reduction and probably generating metallic copper. However, this process is not thought to occur to a great extent in the stoichiometric $CO–O_2$ mixture as Cu^+ carbonyls largely predominate in the spectra when CO is exposed to samples subjected to the reactant mixture (Fig. 3). The following reaction steps are most likely related to an oxidative process. According to EPR results (Fig. 7), this oxidation process passes through an intermediate state in which $O_2^-–Ce^{4+}$ species are formed at the interface. The large decrease of these species at RT suggests that the oxidation process progresses toward the formation of peroxide or, going further, oxide species, with concomitant copper re-oxidation (Fig. 8), thus closing the reaction cycle:

$$\begin{aligned} &Ce^{3+}–V_{\ddot{O}}–Cu^{+}–CO + O_2 \\ &\quad \rightarrow Ce^{4+}–O_2^{-}–Cu^{+}–CO \\ &\quad \rightarrow Ce^{4+}–O_2^{2-}–Cu^{2+} + CO \end{aligned} \quad [3]$$

$$\begin{aligned} &Ce^{4+}–O_2^{2-}–Cu^{2+} + Ce^{3+}–V_{\ddot{O}}–Cu^{+}–CO \\ &\quad \rightarrow 2Ce^{4+}–O^{2-}–Cu^{2+} + CO. \end{aligned} \quad [4]$$

Considering this reaction scheme, the observation of Cu^+ carbonyls under stoichiometric $CO–O_2$ (Fig. 3) indicates that reductive steps [1] and [2] proceed faster than oxidative steps ([3] and [4]). Among the possible single reactions included in [3] and [4], it is probable that those involving oxygen dissociation and/or oxygen migration toward the oxygen vacancies (steps [4]) are the rate-determining steps in the whole process. This hypothesis is consistent with the fact that only vacancies related to cerium ions and not zirconium ions, in contrast to outgassed pure $ZrCeO_4$ (34), are observed upon oxygen adsorption on CuZC reduced at relatively low T_r, suggesting that those oxidative processes could be somewhat limited for the mixed oxide with respect to ceria. Also, the higher intensity of Cu^+ carbonyls shown by CuZC at iso-conversion temperatures (Fig. 2) or in the postreaction experiments (Fig. 3) points in this direction, suggesting that, in spite of the lower reducibility of the copper oxide clusters in CuZC, a greater extent of the reductive process is achieved in this catalyst under reaction conditions due to the slower rate of the oxidative steps in it. Additional support to the hypothesis that reductive steps are not limiting in the process has been observed recently upon comparing CO oxidation activity for pre-reduced and

pre-oxidized Cu/CeO_2 and $Cu/CeO_2/Al_2O_3$ catalysts, which show a lack of dependence on the initial degree of copper reduction (35). It must also be considered that contributions of bulk redox processes, for which the mixed oxide has been shown to be significantly more powerful than ceria (6–12), are unlikely to operate at the low temperatures at which CO oxidation is initiated (13).

It seems unlikely that the different catalytic behavior and redox properties shown by the systems could be attributed to differences in the copper dispersion between the two samples (22). The fact that a similar amount of Cu^{2+} is detected by EPR in both initial samples suggests that similar degrees of dispersion were achieved. Indeed, preliminary XPS results have shown $Cu/Ce = 0.092$ and $Cu/(Ce + Zr) = 0.080$ ratios for the initial calcined CuC and CuZC samples, respectively.

The lower reducibility of copper oxide clusters in sample CuZC may be related to slight structural differences between those species in each sample, as different copper oxide–support epitaxial relationships induced by the different characteristics of the support (lattice parameter and oxygen sublattice structure (23, 34)) are likely to exist. Unfortunately, characterization of such differences is not readily performed. The structureless nature of signal B does not allow conclusions to be extracted of this aspect, while the presence of oxidized copper entities of different types in these samples and the difficulty of avoiding copper reduction induced by the ultravacuum environment or photoionization phenomena in these highly reducible systems also complicate the analysis by XPS. The question is still open in this respect and future investigations will be focused toward its elucidation.

CONCLUSIONS

Two copper catalysts supported on high surface area CeO_2 and $ZrCeO_4$ materials have been comparatively examined with respect to their catalytic activity for CO oxidation.

Correlation between redox properties upon interaction with CO and/or O_2 and catalytic activities indicates that the CO oxidation reaction follows a redox mechanism for both catalysts under which both the active copper entities and the supports are concomitantly reduced or oxidized. On this basis, the reaction mechanism is proposed to involve reductive and oxidative single steps, the rate-determining one being attributed, mainly on the basis of *in situ* DRIFTS results, to the oxidative process.

In agreement with proposals of previous works (17, 18), active copper entities are identified as small copper oxide clusters on the basis of EPR result showing a large facility for reduction–oxidation of those entities.

A higher CO oxidation activity of the CeO_2-supported sample is observed, which is attributed to the higher redox activity of the copper–support interface sites on that catalyst.

ACKNOWLEDGMENTS

A.M.-A. wishes to thank the Comunidad de Madrid for a postdoctoral grant and for financial help under the "Ayudas para estancias breves en centros de investigación extranjeros" program. Projects from CICYT (MAT97-0696-C02-01) and the Comunidad de Madrid (Project 06M/085/96) are acknowledged for financial help.

REFERENCES

1. Trovarelli, A., *Catal. Rev.-Sci. Eng.* **38**, 439 (1996), and references therein.
2. (a) Dictor, R., and Roberts, S., *J. Phys. Chem.* **93**, 5846 (1989). (b) Su, E. C., and Rothschild, W. G., *J. Catal.* **99**, 506 (1986).
3. (a) Shido, T., and Iwasawa, Y., *J. Catal.* **136**, 493 (1992). (b) Shido, T., and Iwasawa, Y., *J. Catal.* **141**, 71 (1993).
4. Martínez-Arias, A., Soria, J., Conesa, J. C., Seoane, X. L., Arcoya, A., and Cataluña, R., *J. Chem. Soc. Faraday Trans.* **91**, 1679 (1995).
5. (a) Yao, H. C., and Yu Yao, Y. F., *J. Catal.* **86**, 254 (1984). (b) Engler, B., Koberstein, E., and Schubert, P., *Appl. Catal.* **48**, 71 (1989). (c) Miki, T., Ogawa, T., Haneda, M., Kakuta, N., Ueno, A., Tateishi, S., Matsuura, S., and Sato, M., *J. Phys. Chem.* **94**, 6464 (1990).
6. Fornasiero, P., Di Monte, R., Ranga Rao, G., Kašpar, J., Meriani, S., Trovarelli, A., and Graziani, M., *J. Catal.* **151**, 168 (1995).
7. Fornasiero, P., Balducci, G., Di Monte, R., Kašpar, J., Sergo, V., Gubitosa, G., Ferrero, A., and Graziani, M., *J. Catal.* **164**, 173 (1996).
8. Balducci, G., Kašpar, J., Fornasiero, P., Graziani, M., Saiful Islam, M., and Gale, J. D., *J. Phys. Chem. B* **101**, 1750 (1997).
9. Trovarelli, A., Zamar, F., Llorca, J., De Leitemburg, C., Dolcetti, G., and Kiss, J. T., *J. Catal.* **169**, 490 (1997).
10. Colón, G., Pijolat, M., Valdivieso, F., Vidal, H., Kašpar, J., Finocchio, E., Daturi, M., Binet, C., Lavalley, J. C., Baker, R. T., and Bernal, S., *J. Chem. Soc. Faraday Trans.* **94**, 3717 (1998).
11. Fornasiero, P., Kašpar, J., Sergo, V., and Graziani, M., *J. Catal.* **182**, 56 (1999).
12. Overbury, S. H., Huntley, D. R., Mullins, D. R., and Glavee, G. N., *Catal. Lett.* **51**, 133 (1998).
13. Kundakovic, Lj., and Flytzani-Stephanopoulos, M., *J. Catal.* **179**, 203 (1998).
14. Vlaic, G., Di Monte, R., Fornasiero, P., Fonda, E., Kašpar, J., and Graziani, M., *J. Catal.* **182**, 378 (1999).
15. Yashima, M., Arashi, H., Kakihana, M., and Yoshimura, M., *J. Am. Ceram. Soc.* **77**, 1067 (1994).
16. Yashima, M., Morimoto, K., Ishizawa, N., and Yoshimura, M., *J. Am. Ceram. Soc.* **76**, 1745 (1993).
17. Liu, W., Sarofim, A. F., and Flytzani-Stephanopoulos, M., *Chem. Eng. Sci.* **49**, 4871 (1994).
18. Luo, M.-F., Zhong, Y.-J., Yuan, X.-X., and Zheng, X.-M., *Appl. Catal. A* **162**, 121 (1997).
19. Martínez-Arias, A., Soria, J., Cataluña, R., Conesa, J. C., and Cortés Corberán, V., *Stud. Surf. Sci. Catal.* **116**, 591 (1998).
20. Martínez-Arias, A., Fernández-García, M., Soria, J., and Conesa, J. C., *J. Catal.* **182**, 367 (1999).
21. Skårman, B., Wallenberg, L. R., Larsson, P.-O., Andersson, A., Bovin, J.-O., Jacobsen, S. N., and Helmersson, U., *J. Catal.* **181**, 6 (1999).
22. Luo, M.-F., and Zheng, X.-M., *Acta Chem. Scand.* **52**, 1183 (1998).
23. Martínez-Arias, A., Fernández-García, M., Ballesteros, V., Salamanca, L. N., Conesa, J. C., Otero, C., and Soria, J., *Langmuir* **15**, 4796 (1999).
24. Hollins, P., *Surf. Sci. Rep.* **16**, 51 (1992).

25. Lokhov, Y. A., Sadykov, V. A., Tikhov, S. F., and Popovskii, V. V., *Kinet. Katal.* **26**, 177 (1985).
26. Davydov, A. A., *Kinet. Katal* **26**, 157 (1985).
27. Padley, M. B., Rochester, C. H., Hutchings, G. J., and King, F., *J. Catal.* **148**, 438 (1994).
28. Kohler, M. A., Cant, N. W., Wainwright, M. S., and Trimm, D. L., *J. Catal.* **117**, 188 (1989).
29. Martínez-Arias, A., Cataluña, R., Conesa, J. C., and Soria, J., *J. Phys. Chem. B* **102**, 809 (1998).
30. Soria, J., Martínez-Arias, A., Martínez-Chaparro, A., Conesa, J. C., and Schay, Z., *J. Catal.* **190**, 352 (2000).
31. Mehran, F., Barnes, S. E., Chandrashekhar, G. V., Mc Guire, T. R., and Shafer, M. W., *Solid State Commun.* **67**, 1187 (1988).
32. Soria, J., Martínez-Arias, A., and Conesa, J. C., *J. Chem. Soc. Faraday Trans.* **91**, 1669 (1995).
33. Fernández-García, M., Martínez-Arias, A., Salamanca, L. N., Coronado, J. M., Anderson, J. A., Conesa, J. C., and Soria, J., *J. Catal.* **187**, 474 (1999).
34. Martínez-Arias, A., Fernández-García, M., Belver, C., Conesa, J. C., and Soria, J., *Catal. Lett.* **65**, 197 (2000).
35. Soria, J., Martínez-Arias, A., Conesa, J. C., Cataluña, R., Palacios, J. M., and Coronado, J. M. (in preparation).